High performance capsule implosions on the OMEGA Laser facility with rugby hohlraums[a)]

H. F. Robey,[1,b)] P. Amendt,[1] H.-S. Park,[1] R. P. J. Town,[1] J. L. Milovich,[1] T. Döppner,[1] D. E. Hinkel,[1] R. Wallace,[1] C. Sorce,[1] D. J. Strozzi,[1] F. Philippe,[2] A. Casner,[2] T. Caillaud,[2] O. Landoas,[2] S. Liberatore,[2] M.-C. Monteil,[2] F. Séguin,[3] M. Rosenberg,[3] C. K. Li,[3] R. Petrasso,[3] V. Glebov,[4] C. Stoeckl,[4] A. Nikroo,[5] and E. Giraldez[5]
[1]*Lawrence Livermore National Laboratory, Livermore, California 94550, USA*
[2]*CEA, DAM, DIF, F-91297 Arpajon, France*
[3]*Plasma Science and Fusion Center, Massachusetts Institute of Technology, Cambridge, Massachusetts 02139, USA*
[4]*Laboratory for Laser Energetics, University of Rochester, Rochester, New York 14623, USA*
[5]*General Atomics, San Diego, California 92186, USA*

(Received 20 November 2009; accepted 8 February 2010; published online 27 April 2010)

Rugby-shaped hohlraums have been proposed as a method for x-ray drive enhancement for indirectly driven capsule implosions. This concept has recently been tested in a series of shots on the OMEGA laser facility [T. R. Boehly, D. L. Brown, R. S. Craxton *et al.*, Opt. Commun. **133**, 495 (1997)]. In this paper, experimental results are presented comparing the performance of D_2-filled capsules between standard cylindrical Au hohlraums and rugby-shaped hohlraums. The rugby hohlraums demonstrated 18% more x-ray drive energy as compared with the cylinders, and the high-performance design of these implosions (both cylinder and rugby) also provided $\approx 20\times$ more deuterium (DD) neutrons than any previous indirectly driven campaign on OMEGA and $\approx 3\times$ more than ever achieved on NOVA [E. M. Campbell, Laser Part. Beams **9**, 209 (1991)] implosions driven with nearly twice the laser energy. This increase in performance enables, for the first time, a measurement of the neutron burn history and imaging of the neutron core shapes in an indirectly driven implosion. Previous DD neutron yields had been too low to register this key measurement of capsule performance and the effects of dynamic mix. A wealth of additional data on the fuel areal density from the suite of charged particle diagnostics was obtained on a subset of the shots that used D ^{3}He rather than D_2 fuel. Comparisons of the experimental results with numerical simulations are shown to be in very good agreement. The design techniques employed in this campaign, e.g., smaller laser entrance holes and hohlraum case-to-capsule ratios, provide added confidence in the pursuit of ignition on the National Ignition Facility [J. D. Lindl, P. Amendt, R. L. Berger *et al.*, Phys. Plasmas **11**, 339 (2004)]. © *2010 American Institute of Physics*. [doi:10.1063/1.3360926]

I. INTRODUCTION

In the indirect-drive approach to inertial confinement fusion (ICF), a high-Z radiation enclosure (or hohlraum) is used to convert incident laser light into x rays to uniformly irradiate a capsule placed at the hohlraum center. The vast majority of previous experiments employed hohlraums of cylindrical shape.[1–3] Recently, there has been increasing interest in hohlraums of an elliptical or "rugby" shape,[4–7] as this design provides the possibility of reduced energy losses into the wall and therefore enhanced radiation drive for a given laser energy input. These hohlraums are currently being investigated for a number of inertial confinement fusion applications. Early experiments on the Laser MegaJoule (LMJ),[8] for example, will use a two laser-cone irradiation scheme (per side), for which a rugby hohlraum shape has several advantages.[4,5] Rugby hohlraums have also been proposed for the implosion of a double-shell capsule[7] on the National Ignition Facility (NIF),[9] and they are also being considered for the Laser Inertial Fusion Energy program.[10]

The advantage of the rugby hohlraum shape can be easily seen by considering an energy balance in the hohlraum. Following Lindl,[9] we can write down the energy balance between sources and sinks as

$$\eta_{ce} \cdot E_{\text{laser}} = E_{\text{wall}} + E_{\text{LEH}} + E_{\text{capsule}} = f(T_R^4, A_{\text{wall}}, A_{\text{LEH}}, A_{\text{capsule}}, \tau), \quad (1)$$

where E_{laser} is the incident laser energy, E_{wall} is the energy lost to the hohlraum wall with area A_{wall}, E_{LEH} is the energy lost out of the laser entrance holes (LEH), and E_{capsule} is the energy absorbed by the capsule. Here, η_{ce} is the conversion efficiency from laser energy to x rays, and T_R is the steady-state radiation temperature attained for a constant power laser pulse of duration τ. As an example, consider the comparison of hohlraum shapes shown in Fig. 1, which compares a cylinder and a rugby with the same equatorial and LEH diameters. As a specific example, let us consider the dimensions of the design presented in Ref. 11. The areas of the wall, capsule, and LEH are summarized in Table I.

The peak T_R obtained from Eq. (1) in the rugby is predicted to be 245 eV versus a peak of only 229 eV for the

[a)]Paper XI2 4, Bull. Am. Phys. Soc. **54**, 343 (2009).
[b)]Invited speaker.

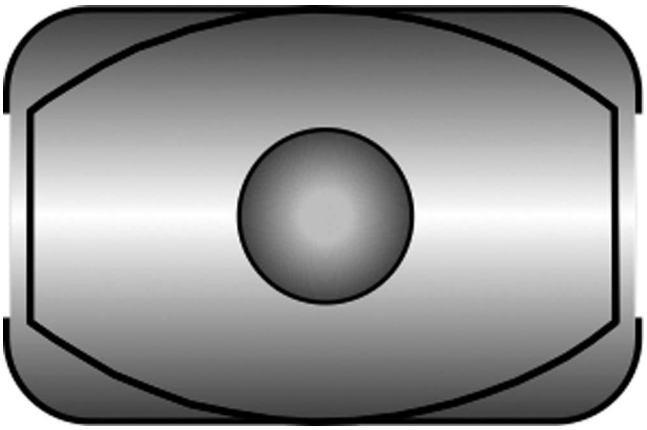

FIG. 1. Drawing comparing the relative dimensions of a rugby and cylindrical hohlraum.

cylinder. This corresponds to a 31% increase in the radiation flux between the two hohlraums.

There is clearly a significant additional energy loss to the wall in the corners of the cylindrical hohlraum. The corner radius of the cylinder used in this estimate is that of an OMEGA "scale-1" hohlraum, r_{corner}=150 μm, which is 19% of the hohlraum radius at the equator. The corresponding ratio in the rugby, by comparison, is 1.0, as the wall contour is by definition[11] an arc of a circle. It is interesting to compare these relative corner radii with those of a candidate NIF ignition hohlraum with corner and hohlraum radii of 1.2 and 2.72 mm, respectively (giving a ratio of 0.44).[12] Increasing the corner radius of the OMEGA-scale cylinder of Fig. 1 to 44% of the hohlraum radius (r_{corner}=352 μm) raises the peak T_R to 235 eV, which is still 19% lower flux than the rugby design. The NIF design therefore falls in between the two cases considered here with a smaller relative energy loss in the corners than the Omega-scale cylinder but a greater relative energy loss than in a rugby design.

Recently, a numerical design study comparing the performance of traditional cylindrical versus rugby hohlraums was presented.[11] In this study, a high performance implosion design was presented, which predicted a substantial increase in drive in the rugby hohlraum. The performance predictions of Ref. 11 were recently tested in a series of experiments on the OMEGA laser facility[13] at the Laboratory for Laser Energetics (LLE), University of Rochester. Details of the experiment and an overview of the experimental results have been recently reported in Ref. 6. The goal of these experiments was twofold. First, the high-performance design of *both* hohlraum styles, with larger capsules and smaller LEH diameters, promised a sufficient increase in the neutron yield to access additional neutron diagnostics, which heretofore have not been accessible using indirect drive. Second, these experiments were the first direct comparison of cylindrical versus rugby hohlraums and provide an opportunity to demonstrate the predicted drive advantage of rugby hohlraums. It is very important to note, however, that in order to make the most direct comparison of the relative hohlraum drive differences, identical capsules were used in both hohlraums. The capsule choice was optimized for the cylindrical hohlraums, and when the same capsule is used in the rugby hohlraum, it is overdriven resulting in less than optimal performance.

TABLE I. Comparison of capsule, wall, and LEH dimensions for a cylinder vs rugby hohlraum.

Parameter	Rugby	Cylinder
Hohlraum length (μm)	2275	2450
Hohlraum radius (μm)	800	800
LEH aperture (%)	50	50
Hohlraum corner radius (μm)	800	150
Area LEH (x2) (mm^2)	1.0	1.0
Area capsule (mm^2)	0.67	0.67
Area wall (mm^2)	9.6	13.9

FIG. 2. Photographs of the targets, axial and side views.

Both of these goals were successfully met. As reported in Ref. 6, record indirectly driven DD neutron yields in excess of 10^{10} were achieved, in very good agreement with preshot simulations[11] for both cylindrical and rugby hohlraums. This yield increase enabled the first demonstration of both a neutron imaging system developed by the Commissariat à l'Energrie Atomique (CEA)[14] and the LLE neutron temporal diagnostic (NTD),[15,16] which provides a temporal history of the neutron production. In this paper, the results of these experiments are presented together with comparisons with postshot numerical simulations.

II. EXPERIMENTAL PARAMETERS

Figure 2 shows photographs of the targets used in the experiments. The axial view shown on the left is essentially identical for both hohlraums. The diameters of the equator, the LEH, and the capsule are the same for both hohlraums. The side view shows the tapered wall of the rugby hohlraum. The square feature seen in the center of both side views is a thin CH patch overcoated with 2 μm of Au. This patch cov-

TABLE II. Summary of capsule parameters.

	Shot											
	54734	54735	54736	54738	54739	54740	54741	54744	54745	54746	54747	54748
Hohlraum	rugby	rugby	rugby	rugby	rugby	rugby	rugby	cyl	cyl	cyl	cyl	cyl
OD (μm)	643.4	650.4	654.2	650.8	650.6	655.8	664.8	647.4	668.4	645.4	657.4	647.0
ID (μm)	548	553	561	559	555	549	556	551	566	553	567	550
Ge-layer (μm)	35.3	36.3	34.2	33.5	35.4	41	42	35.8	38.8	33.8	32.8	36.1
Total wall (μm)	47.7	48.7	46.6	45.9	47.8	53.4	54.4	48.2	51.2	46.2	45.2	48.5
Gas	DD	DD	DD	DD	D ^{3}He	D ^{3}He	D ^{3}He	D ^{3}He	D ^{3}He	DD	DD	DD
Pr (atm)	10	10	50	50	50	50	50	50	50	50	50	50

ers a 300 μm diameter diagnostic hole to enable viewing of the x-ray emission from the imploded core of the capsule.

The capsule shells used in these experiments consisted of a 9.8 μm thick CH (polystyrene) mandrel, a 2.6 μm thick polyvinyl acetate (PVA) layer, and a 2.7% Ge-doped CH layer of variable thickness. Table II summarizes the hohlraum type, capsule inside diameter (ID), outside diameter (OD), Ge-doped layer thickness, total wall thickness, gas-fill species, and gas-fill pressure for each capsule.

Seven of the capsules used pure deuterium (D_2) fuel at fill pressures of 50 and 10 atm to test the role of convergence and increasing effects of interfacial mixing. The remaining five capsules used D ^{3}He fuel to access the suite of charged particle diagnostics.

The hohlraums were all driven with 40 beams of OMEGA with 20 beams directed into each LEH. The laser pulse shape duration was 1 ns with a nominally constant power/beam of 0.5 TW. The total laser energy on target was very repeatable from shot-to-shot with an average laser energy of 19.62 ± 0.17 kJ. Distributed phase plates of elliptical shape (E-IDI-300) (Ref. 17) with a nominal 300 μm spot width were used for beam smoothing. With the small LEH diameters used in these experiments, there was some concern over clipping of the beams at the LEH opening. The x-ray emission from the LEH was monitored on each shot with a gated x-ray framing camera, and no clipping was observed. No smoothing by spectral dispersion[18] or polarization smoothing using distributed polarization rotators[19] was used in order to maximize the laser energy delivered to the hohlraum. Figure 3 shows the nominal pointing of the three cones of beams at angles of 23.2° (cone 1), 42° (cone 2), and 58.9° (cone 3) in the two hohlraums. The beam pointing and defocus values, relative to the center of each LEH, are identical. Since the rugby hohlraum is 175 μm shorter in length than the cylinder, cone 1 beams pass the capsule in slightly closer proximity than in the cylinder. An important difference is noted in the cone 3 beams as well. Due to the tapered shape of the rugby wall near the LEH, the cone 3 beams intercept the wall at an axial position closer to the LEH than in the cylinder. Note also that the cone 3 beam spots on the hohlraum wall in the rugby are considerably larger than in the cylinder. These beams will therefore pass through a longer path length of ablated Au plasma than in the cylinder. This will be of importance when we consider the backscatter data in Sec. IV.

III. EXPERIMENTAL CONFIRMATION OF RUGBY DRIVE ENHANCEMENT

In Ref. 6, an extensive summary and discussion of the neutron yields from these experiments was presented. We will not further elaborate on these results except to reiterate that the design of these implosions did indeed result in the highest yield ever reported in an indirectly driven implosion with D_2 fuel. The yields of both the rugby (1.29×10^{10} and 1.51×10^{10}) and cylinder (1.22×10^{10} and 1.37×10^{10}) were approximately 20 times greater than the previous OMEGA record of 8×10^8 and 3× greater than the NOVA record of 4×10^9, which was achieved with 32 kJ of laser energy input as compared to the 19.5 kJ used in these experiments. The error on the neutron yield measurement is 1.5% or 2×10^8 in all cases. We note also that the measured yields showed relatively little difference between rugby and cylinders as predicted.[11] It is important to note, however, that the symmetry and capsule thickness tuning was considerably better in the cylinders, as will be demonstrated.

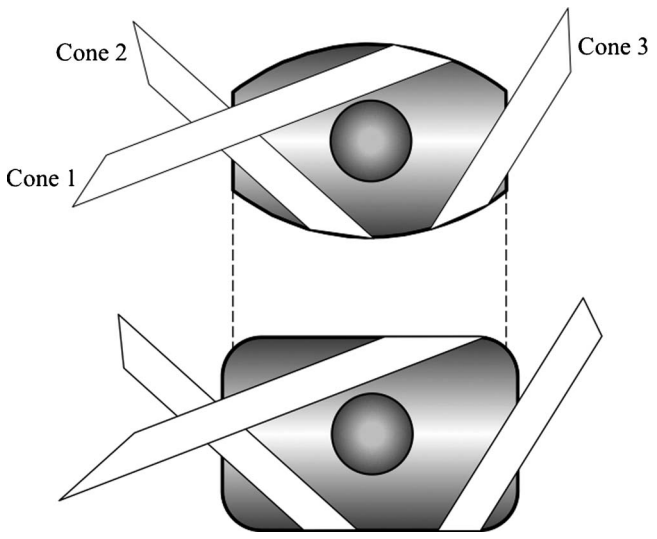

FIG. 3. Drawing showing the pointing of the three beam cones in rugby vs cylindrical hohlraums.

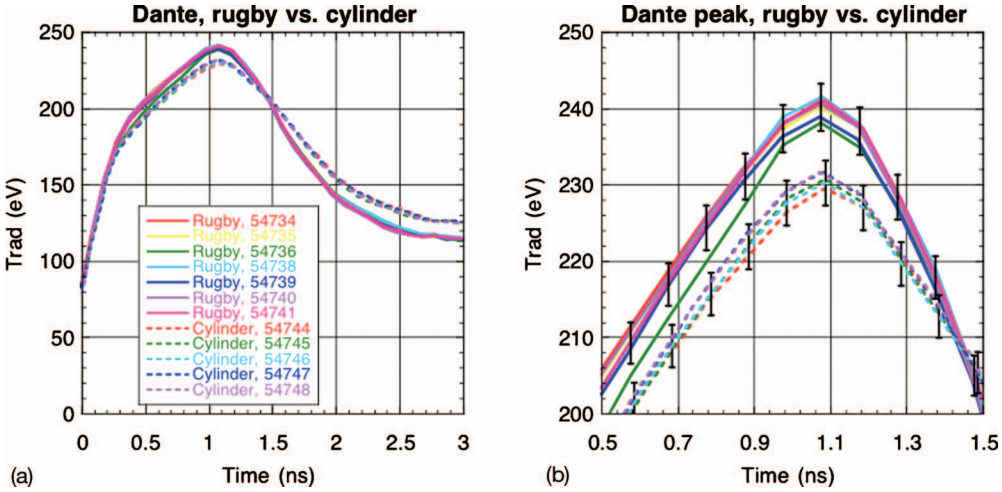

FIG. 4. (Color) (a) Measured Dante radiation temperature history for all shots. (b) Detailed T_R history at the peak.

We now turn our attention to the drive advantage of rugby hohlraums. Figure 4(a) shows the full radiation drive history (0 to 2 keV) as measured by Dante[20] for all of the shots. Figure 4(b) gives the details near the time of peak x-ray drive and includes error bars of $\pm 1.3\%$ from Ref. 20 for the relative shot-to-shot error in T_R. The absolute error bars on the Dante measurement are larger ($\pm 5\%$) from the calibration measurements reported in Ref. 21, and will be discussed later in comparison with numerical simulations presented in Sec. V. As can be seen, the repeatability of the data is very good and clearly demonstrates a consistent 10 eV increase in the rugby hohlraums. Comparing this peak drive with the energetics estimates presented in Sec. I, we see that the peak T_R in the cylinders is very close to that predicted, whereas the peak T_R in the rugby is about 5 eV lower than that predicted by the energy balance. If we include a 10% backscattered energy loss in the rugby hohlraum, this brings the energetics estimate into agreement with the measurements. In Sec. IV, it will be shown that this estimate is consistent with observations from a wide range of additional diagnostics of the implosion performance. It is also important to note that the temperature estimated in Sec. I is the average internal T_R, whereas the Dante measurements of Fig. 4 give an estimate of T_R derived from the flux viewed through the LEH at an angle of 37°. Due to the different areas of the wall viewed, these two quantities are not necessarily the same.

A very important (and independent, target-center based) confirmation of this drive increase is obtained from the charged particle diagnostics. Two types of charged particle diagnostics were used on these shots, with up to three fielded from different viewing angles on a single shot as shown in Fig. 5. Spatially resolving CR39 nuclear track detectors[22] were used to obtain images of the proton fluence, and spectrally resolving wedge range filters (WRFs) (Ref. 22) were used to obtain spectra of the downscattered protons versus position. The CR39 measurements shown in Fig. 5(b), which are extensively discussed in Ref. 23, showed considerable anisotropy when viewed through the LEH, but were reasonably isotropic when viewed from the equator. For this reason, we will focus on results obtained from diagnostic orientations viewing the equator. The WRFs record the spectrum of protons originating from the reaction of $D+{}^3He->p(14.7\ MeV)+\alpha(3.6\ MeV)$ and characteristically show protons generated in two episodes, one at shock convergence at the origin (shock flash) and one at peak compression. Figure 5(a) shows a typical example of the downscattered spectrum. The shock flash peak at about 13 MeV is due to protons generated at shock stagnation (when the fuel and capsule areal density is still low), and the broader peak centered at 11 MeV is due to the downshift of protons generated at peak compression, which traverse higher capsule areal density. Figure 5(c) compares the energy downshift, corrected for the energy loss of the protons passing through the 25 μm Au hohlraum wall, for both rugby and cylinder at several viewing orientations. Several observations can be made. First, we note that the variation as a function of position from equator to pole and back to equator is reasonably uniform. Second, the shock-flash generated protons show very little variation between the two hohlraums. This occurs because the shock flash occurs prior to any significant shell convergence, at which time the capsules in the rugby and cylinder have very similar areal densities, in agreement with the preshot simulations of Ref. 11.

We now compare the results for the compressional down shift in the cylindrical hohlraums. The downshift increases with increasing areal density ρR as can be seen for the two initial ablator thicknesses shown for the cylinders. An increase of 3 μm in the initial ablator thickness corresponds to an additional 0.4 MeV increase in the proton energy downshift. Next we compare the results for the 48.2 μm thick ablator in a cylinder with a very similar 47.8 μm thick ablator in a rugby hohlraums. The measured energy downshift in the rugby is 0.8 MeV lower than the results for the cylinder with comparable ablator thickness. This is significantly greater than the ± 0.15 MeV error bars on the measurement,[22] and based on the observation from the cylinders, this implies an additional 6 μm of ablated mass in the rugby hohlraum. This increase in mass ablation in the

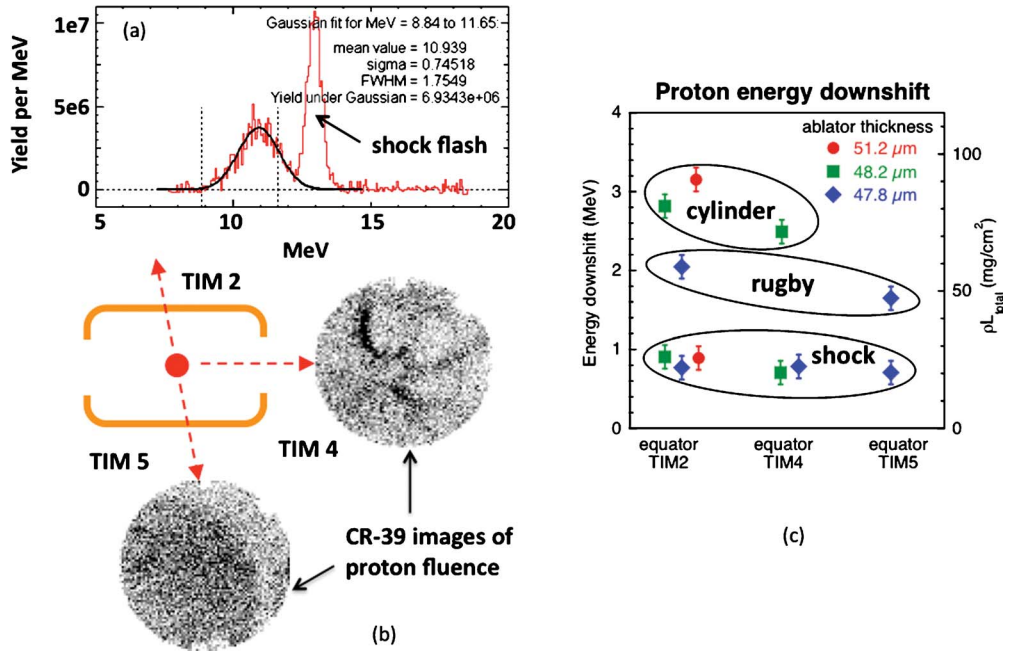

FIG. 5. (Color online) (a) Downscattered proton spectrum for a D ^{3}He-filled capsule showing the shock flash generated protons at 13 MeV and compressional protons centered at 11 MeV. (b) Spatial images of proton fluence (c) Comparison of proton energy downshift between rugby and cylinder at several viewing orientations.

rugby hohlraums serves as a capsule-centric confirmation of the enhanced drive, and again confirms the predictions given in Ref. 11.

IV. ADDITIONAL EXPERIMENTAL OBSERVATIONS

A number of additional diagnostics were used on these shots as well, and while all returned high quality data, several observations were not in agreement with preshot simulations. Figure 6, for example, gives a summary of the measured neutron bang times for each of the shots. The error bars on the data are ±50 ps from the shots where good NTD data were obtained, and ±100 ps on shots where the bang time is measured with the less sensitive NBT detector.[24] From preshot simulations,[11] it was expected that the x-ray bang times in the rugby hohlraums would be earlier by about 200 ps than in the cylinders due to the increase in drive. For the 50 atm D_2-filled capsules, for example, the bang time was predicted to be 1.7 ns in rugby hohlraums versus 1.9 ns in cylinders. Including information about the as-shot capsule thicknesses, the bang times for the cylinders are in reasonable agreement with preshot simulations, while those for the rugby hohlraums are consistently late.

X-ray core emission images were obtained on all of the shots providing information about the implosion symmetry. Figure 7(a) shows images of the core emission from both D_2-filled and D ^{3}He-filled capsules in the two hohlraums. The emission was recorded with a gated x-ray framing camera[25] through a 300 μm diagnostic hole in the side of the hohlraum. The hole was covered with a 20 μm CH patch overcoated with 2 μm of Au on the interior side to maintain the hohlraum albedo. The images shown in Fig. 7(a) are 230×230 μm^2 in extent, and in all cases the hohlraum axis is vertical. The examples of Fig. 7(a) are fully representative of all shots, where the implosion core shapes were consistently more "pancaked" (or oblate) in the rugby hohlraums. Preshot simulations of Ref. 11 predicted that the core emission would be ~20% larger in the rugby hohlraums. Lineouts of emission profiles taken along the hohlraum axis in Fig. 7(a), however, demonstrate that the width of the core emission (full width at half maximum) is very similar for both hohlraums. It is only in the perpendicular direction, in

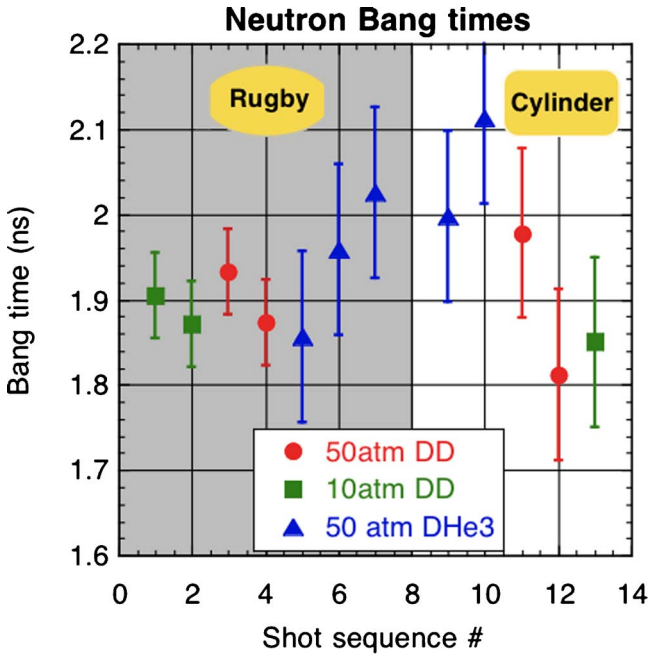

FIG. 6. (Color online) Measured neutron bang times for all shots. Error bars are ±50 ps for NTD data, ±100 ps for NBT data.

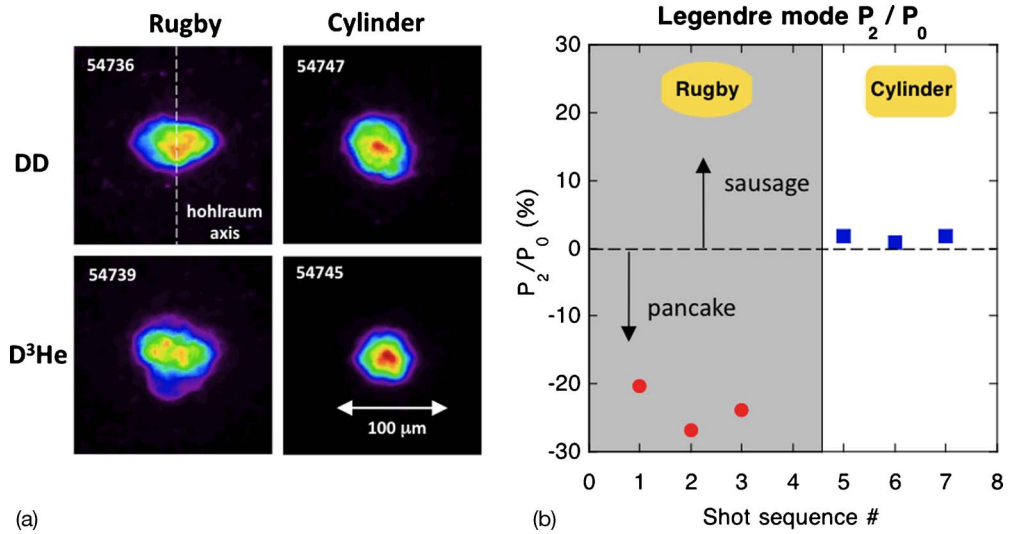

FIG. 7. (Color online) (a) Temporally gated x-ray emission core images for 50 atm D_2-filled and 50 atm D ^{3}He-filled capsules in both rugby and cylindrical hohlraums. Hohlraum orientation is vertical in all images. (b) Summary of normalized second Legendre polynomial coefficients P_2/P_0 for a 10 atm D_2 (sequence nos. 1 and 7), 50 atm DD (nos. 2 and 6), and 50 atm D ^{3}He-filled (nos. 3 and 5) capsules in (rugby, cylindrical) hohlraums.

the plane of the equator, that the width of the emission is approximately 50% larger in the rugby hohlraums.

Figure 7(b) quantifies the core symmetry by plotting the normalized Legendre polynomial coefficient P_2/P_0 extracted from an analysis of the 50% emission contour taken at the time of peak x-ray emission. For each hohlraum type, the Legendre mode coefficient is shown for a 10 atm D_2, a 50 atm D_2, and a 50 atm D ^{3}He-filled capsule. The symmetry is very good for all implosions in cylinders and consistently pancaked in all of the rugbys with $P_2/P_0 = -20\%$ to -28%.

The reason for the change in symmetry becomes apparent when one looks at the data from the backscatter diagnostics. Figure 8 shows the data from the full aperture backscatter station (FABS) diagnostic,[26] which was fielded on one of the cone 3 beams (no. 25). The location of beam 25 on the hohlraum wall is shown in the inset for each case. In all shots, backscattered energy from stimulated Brillouin scattering (SBS) was observed, while no measurable stimulated Raman scattering (SRS) was seen on any of the shots. In addition, the near backscatter imager (NBI) diagnostic[27] was fielded, but in all cases less than 10% additional energy above that seen by the FABS was recorded. Figure 8(a) shows that the backscattered energy was very consistent within shots with a given hohlraum shape. The average backscattered energy was 7.2% in the rugby hohlraums and 1.3% in the cylinders. The variation within the rugby hohlraums is even more consistent, when one notes that the first shot had a slightly different focus location for the cone 1 and cone 3 beams than the remaining six shots. Between shots 1 and 2, the focus of cone 1 was moved from the center of the LEH to a position 400 μm inside the LEH. The focus of the cone 3 beams was also moved inward from 1450 to 650 μm outside of the LEH. This change in beam focus toward the hohlraum interior was made after observation of the core symmetry in

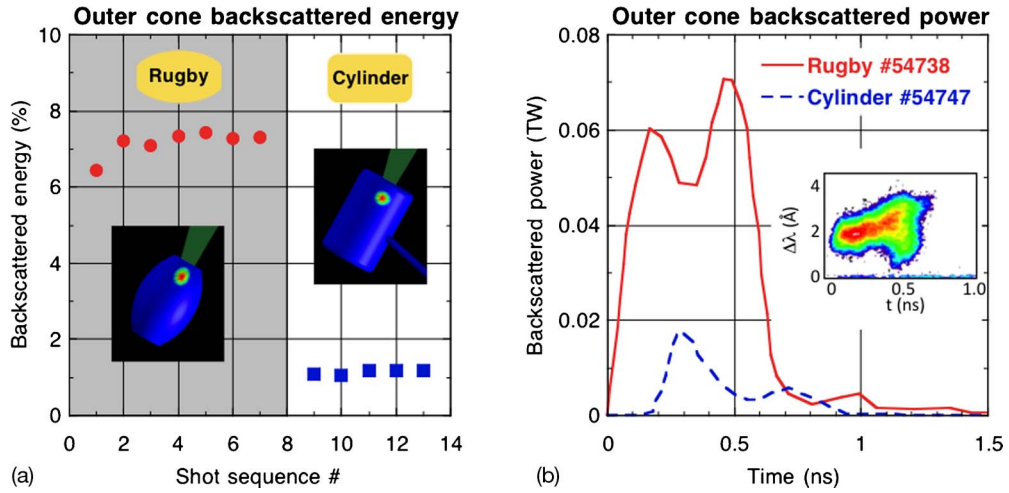

FIG. 8. (Color online) (a) Summary of measured outer cone (no. 3) backscattered energy vs shot sequence. Rugby (circles) and cylinder (squares). Inset shows the location of the cone 3 FABS beam on each hohlraum wall. (b) Comparison of measured outer-cone backscattered power for rugby (solid line) and cylinder (dashed line). Inset shows FABS streaked image of wavelength shift vs time.

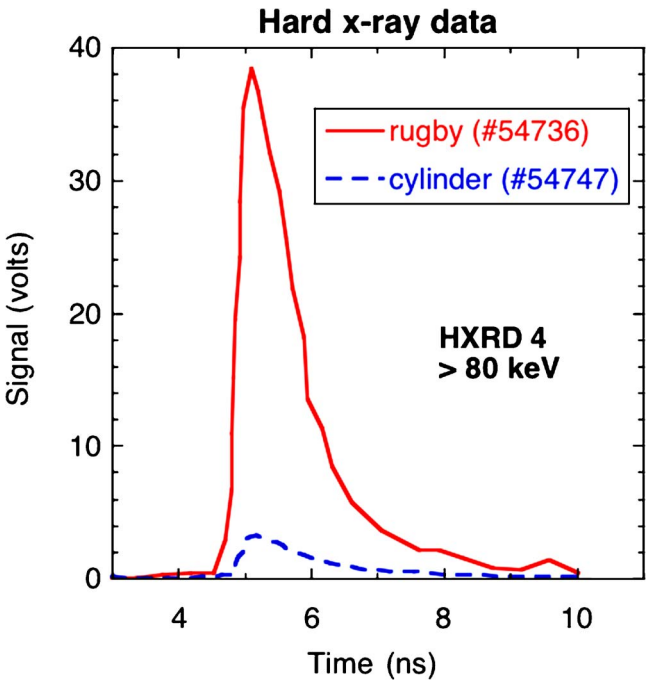

FIG. 9. (Color online) Comparison of HXRD data for channel 4 ($E>80$ keV photons) for rugby (solid line) and cylinder (dashed line). Absolute time reference is arbitrary.

the first shot, where it was suspected that the beams were possibly clipping on the rather small LEH opening. This focal change caused a very consistent 10% increase in the backscatter level.

Figure 8(b) shows the corresponding backscattered power history comparison between a rugby and cylindrical hohlraum. In both cases, the backscatter is observed early in the pulse. For the rugby, it is significant for the first 600 ps of the pulse and negligible thereafter. The inset shows the FABS streak image for the rugby hohlraum. The wavelength shift is approximately 2 Å, which is in excellent agreement with preshot predictions[11] for scattering from ablated Au. Scattering from ablated capsule material will give a larger wavelength shift and will be important for the inner cones.

A related measurement is obtained from the hard x-ray detector (HXRD),[28] which is a strongly filtered four-channel array of x-ray diodes recording hohlraum emission of x-ray photons above 20, 40, 60, and 80 keV, respectively. For the present series of shots, only two channels (1 and 4) of this detector were operational. Figure 9 shows a comparison of the 80 keV channel response for a rugby and a cylinder. The absolute time reference on this plot is arbitrary, as the detector timing was not calibrated for these shots. The hard x-ray signal is approximately 20 times greater in the rugby, indicating that there is likely considerable SRS occurring on the inner cones, which were not measured with the FABS or NBI due to the hohlraum orientation. This observation is consistent with previous measurements in an empty (no capsule) vacuum rugby-like hohlraum experiment reported recently by Casner *et al.*[5] Though the hohlraum shape and beam pointing were slightly different in that experiment, the backscatter was measured to be 5% on cone 2 and 10% (with 5% SRS) on cone 1. No directly comparable results for a cylindrical hohlraum were obtained in those experiments, however. To fully characterize the backscatter difference between a rugby and cylindrical hohlraum, a dedicated measurement of the inner cone backscatter would be needed.

V. COMPARISON WITH NUMERICAL SIMULATION

To briefly summarize the observations in Secs. III and IV, two of the diagnostics gave a clear signature of drive enhancement in rugby hohlraums. (1) An external measurement of the hohlraum radiation flux (Dante) showed a very repeatable 10 eV increase in the peak flux, and (2) a measurement of the energy downshift of 14.7 MeV protons produced at the capsule center demonstrated smaller energy downshifts consistent with enhanced mass ablation in the rugby hohlraum. Several other diagnostics, however, gave results which were not expected from preshot predictions: (1) backscatter was significantly higher in the rugby hohlraums, (2) x-ray core emission in rugby hohlraums was less symmetric than cylinders, and (3) x-ray bang times in rugby hohlraums were later than expected. In order to explore this, postshot simulations have been performed. These simulations include measured laser power histories and as-shot capsule diameters, wall thicknesses, and dopant concentrations. The measured time-dependent outer-cone backscatter is used, and a range of assumed inner-cone backscatter levels is included to assess the effect on all diagnostics.

Table III gives a summary of the postshot simulated yields for both hohlraums. For the cylinder, simulations are performed with (1) no backscatter, (2) the inclusion of the measured cone 3 backscatter, and (3) an additional 1.3% backscatter on both inner cones with the same measured time dependence as for cone 3. As Table III shows, for these small levels of backscatter, there is little variation in the simulated

TABLE III. Comparison of simulated yields and yield-over-clean (YOC) for rugby vs cylindrical hohlraums.

Rugby backscatter	Rugby yield	Rugby YOC (%)	Cylinder backscatter	Cylinder yield	Cylinder YOC
None	2.70×10^{10}	48	None	1.64×10^{10}	83
7.2%, cone 3	2.57×10^{10}	50	1.3%, cone 3	1.57×10^{10}	87
+5% cones 1 and 2	2.50×10^{10}	52	+1.3% cones 1 and 2	1.50×10^{10}	91
+10% cones 1 and 3	2.33×10^{10}	55			
+15% cones 1 and 3	2.15×10^{10}	60			
+20% cones 1 and 3	2.07×10^{10}	62			

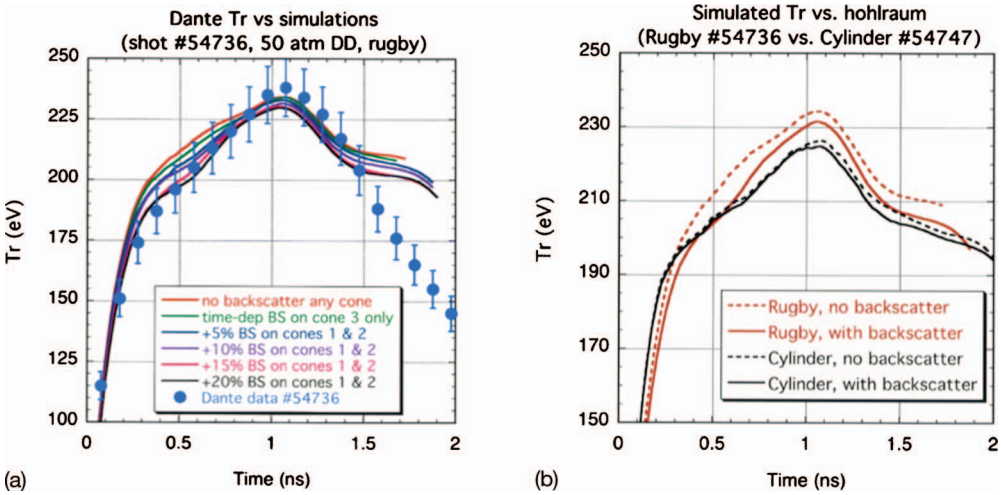

FIG. 10. (Color) (a) Comparison of measured Dante data (shot no. 54736) vs simulated Dante histories from simulations including no backscatter (red), measured cone 3 backscatter only (green), measured cone 3+ an additional 5% (blue), 10% (purple), 15% (magenta), and 20% (black) assumed backscatter loss on both inner cones. (b) Comparison of simulated Dante histories between rugby (red) and cylinder (black). Simulations without backscatter are shown with dashed curves and simulations with backscatter losses are shown with solid curves.

yields, and the ratio of the measured yield over the simulated clean (i.e., no mix) yield ("YOC") is always over 80%, indicating excellent agreement. For the rugby, simulations are again performed with no backscatter, measured outer cone backscatter, and a range of inner cone values from 5% to 20%, all with the same time dependence as that measured for cone 3. From Table III, the simulated yield falls with increasing backscatter, and the YOC increases from 48 to 62%, all in very reasonable agreement with the data.

Turning now to the drive comparison, Fig. 10(a) shows a comparison of the measured Dante for a 50 atm D_2 rugby shot (no. 54736) with the simulated Dante histories for the assumed range of inner cone backscatter. As is seen, due to the time dependence of the backscatter, the simulated drive is most strongly affected in the first half of the pulse. The simulations with at least 10% assumed backscatter on the inner cones are within the ±5% error bars on the Dante data[21] throughout the pulse. The discrepancy between data and simulation for $t > 1.5$ ns is due to incorrect modeling of LEH closure in the simulations, but occurs too late to have any impact on any of the simulated observables.

Figure 10(b) shows a comparison of the simulated drive between the rugby and the cylinder. The red curves are for the rugby hohlraum, and the black curves are for the cylinder. Dashed curves give the simulated Dante in the absence of backscatter, and solid curves give the result with 15% and 1.3% assumed inner-cone backscatter in the rugby and cylinder, respectively. As is seen, there is very little change in the cylinder due to the very small level of the backscatter correction. For the rugby, however, inclusion of backscatter significantly decreases the drive early in time while still achieving a peak T_R that is 7 eV higher than that in the cylinder. This time-dependent drive difference is important, as it explains the bang-time discrepancy noted earlier in Sec. IV.

Figure 11 shows the comparison between the simulated x-ray bang times and the postshot simulations. The simulation with no backscatter (square symbol) is early by nearly 200 ps as compared to the data for shot no. 54736, where we included the more stringent ±50 ps error bars from the NTD measurement. With increasing assumed backscatter (circle symbols) and correspondingly reduced drive, the simulated x-ray bang time is increasingly delayed. The simulations with inner cone backscatter levels of 15%–20% fall within the error bars of the data. This is consistent with the value of >10% that provided agreement between the simulated drive and the Dante data of Fig. 10. The previous observation from Fig. 6 that bang times were similar in rugby and cylindrical hohlraums can now be understood. Inclusion of backscatter

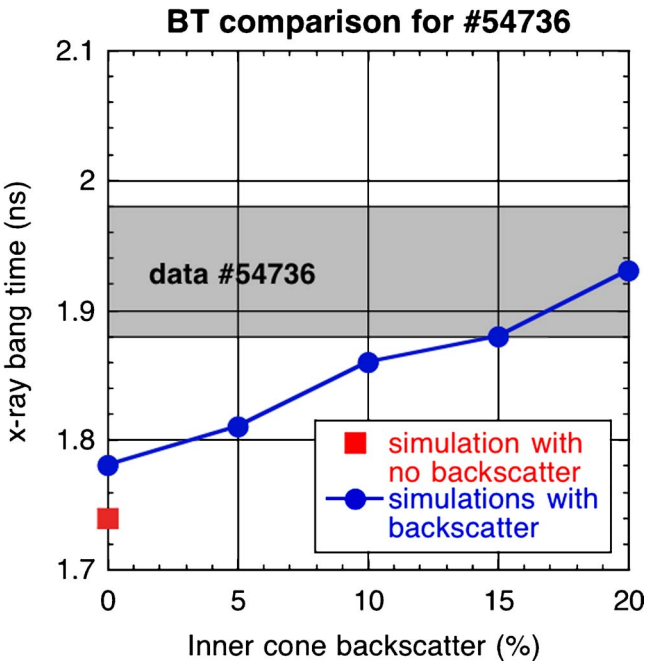

FIG. 11. (Color online) Comparison of measured (shot no. 54736, 50 atm DD-filled rugby) and simulated x-ray bang times vs level of assumed inner cone backscatter.

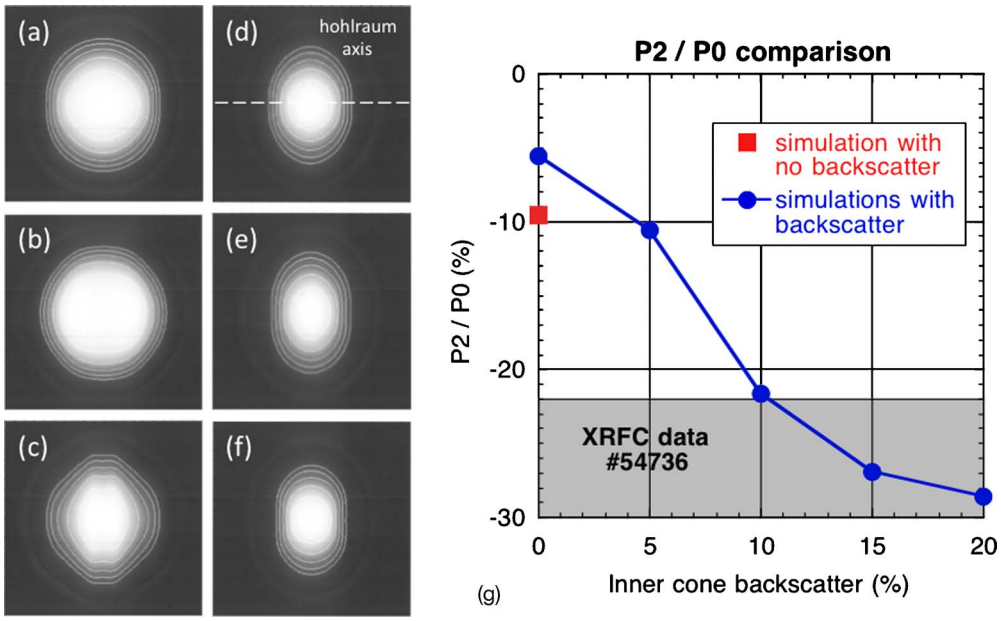

FIG. 12. (Color online) Simulated x-ray core emission images with (a) no backscatter, (b) measured cone 3 backscatter only, measured cone 3 plus an additional 5% (c), 10% (d), 15% (e), and 20% (f) assumed backscatter loss on both inner cones. (g) Comparison between measurement and simulation of normalized second Legendre polynomial coefficient P_2/P_0 vs level of assumed inner cone backscatter.

losses in a rugby decreases the drive early, but still achieves a higher peak flux, resulting in similar bang times.

An assumption of 15% inner cone backscatter is consistent with the x-ray core emission images as well. Figures 12(a)–12(f) show simulated emission images for the range of assumed backscatter on the inner cones. Legendre polynomial coefficients, again extracted from the 50% contour levels, are shown in Fig. 12(g). As before, the simulation with no backscatter is shown with the square symbol, simulation results with assumed inner cone backscatter are shown with circle symbols, and the data with ±5% error bars are shown in gray. The simulation with 15% assumed inner-cone backscatter falls right in the middle of the error bars of the data, further supporting the agreement seen in the Dante and x-ray bang-time comparisons.

Figure 13 shows a comparison of the simulated proton spectra versus the assumed level of inner cone backscatter. Spectra are shown at both the pole (black) and the equator (red). A number of interesting effects are observed in the simulated proton spectra with increasing backscatter. As Fig.

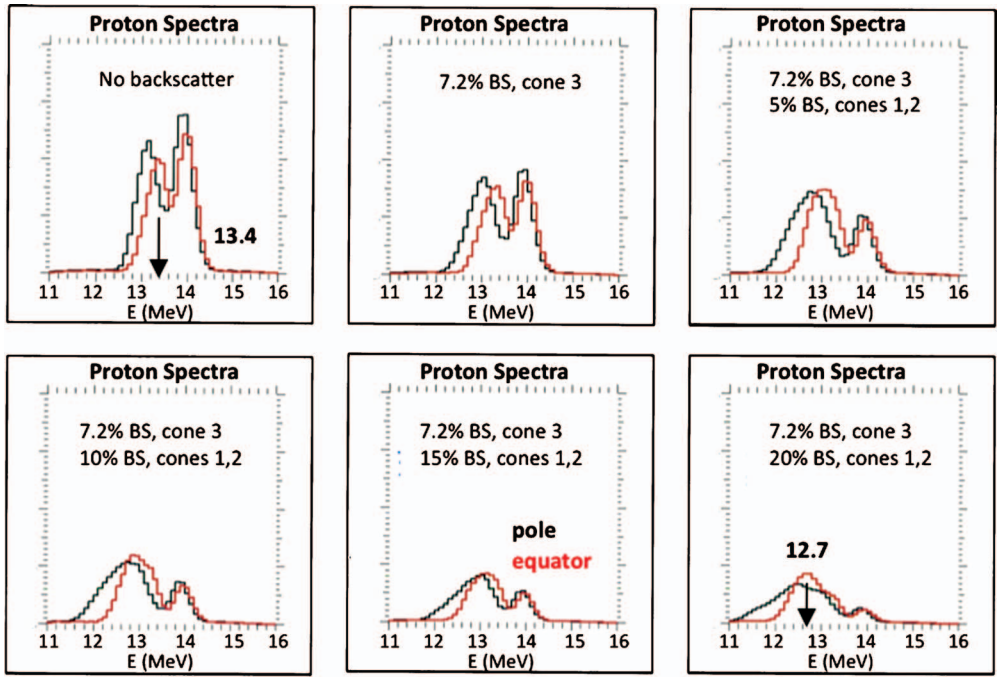

FIG. 13. (Color) Simulated downscattered proton spectra vs level of assumed inner cone backscatter at the pole (black) and equator (red).

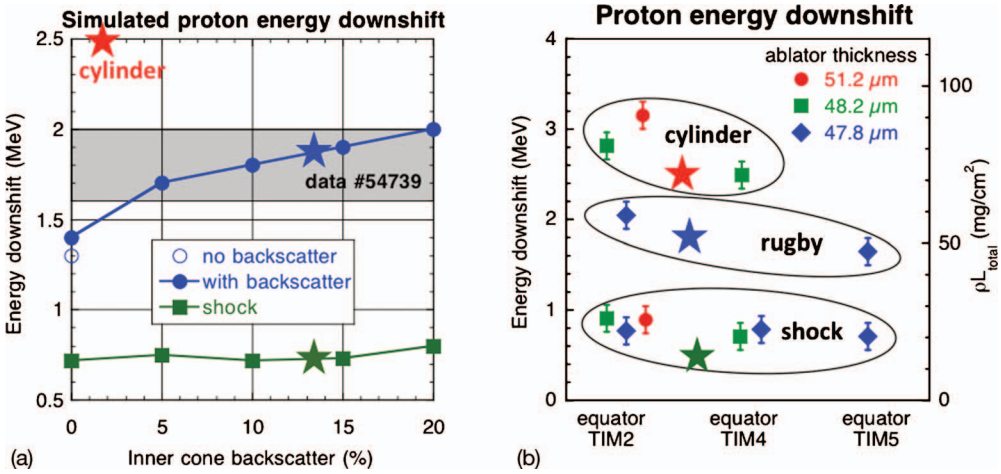

FIG. 14. (Color) (a) Comparison of measured (shot no. 54739, D ^{3}He-filled, rugby) vs simulated proton spectra vs level of assumed inner cone backscatter. Energy downshift of shock flash protons (green), compressional protons in rugby (blue), and compressional protons in cylinder (red). (b) Comparison of simulation vs data. Blue star is rugby simulation with 15% assumed inner cone backscatter. Red star includes 1.3% backscatter on all cones.

13 shows, the total proton yield decreases as a result of the decreased drive, ranging from 3.4×10^7 with no backscatter to 1.3×10^7 with 20% assumed backscatter. Also, the shock-flash-generated protons are observed to decrease at a faster rate than those created at compression. This is due to the very strong temperature dependence of the shock-generated protons, and the decrease in this temperature as the symmetry of the implosion is changed with increasing backscatter on the inner cones. The proton energy downshift of the compressional peak increases with the decrease in drive, as more mass remains at bang time with the reduced drive. With no backscatter, the compressional protons are downshifted with a spectral peak at 13.4 MeV, while the simulation with 20% assumed inner cone backscatter shows a peak of the compressional protons at 12.7 MeV.

Figure 14 quantifies the comparison of the simulated proton spectra with the data of Fig. 5. Figure 14(a) plots the simulated energy downshift for the shock-generated protons (green symbols), the compressional protons in rugby hohlraums (blue), and a single point (red star) for the compressional protons in a cylindrical hohlraum. As with the other diagnostics, the simulation with 15% assumed inner cone backscatter is in excellent agreement with the data (shot no. 54739), where the error bars are taken from the observed angular variation in the data between the two equatorial measurements. The comparison between simulation and the data is shown in Fig. 14(b), where both compressional and shock-flash generated energy downshifts are in excellent agreement with the data for both hohlraums.

VI. SUMMARY AND DIRECTIONS FOR FUTURE WORK

In summary, the first direct comparison of the performance of rugby versus cylindrical hohlraums has been presented. The performance of both with regard to neutron yield was excellent due to the more NIF-like (i.e., smaller LEH diameters and smaller case-to-capsule ratios), high-performance design of the implosions. Record DD neutron yields were obtained in both cases. The rugby hohlraums demonstrated 18% more x-ray drive energy as compared with the cylinders. This drive enhancement was verified both by an external measurement of the hohlraum x-ray radiation flux (Dante) as well as by an internal capsule-centric measurement of the energy downshift of protons in D ^{3}He-filled capsules.

SBS backscatter was observed to be significantly higher in the rugby hohlraums. This affected the implosion symmetry, the measured x-ray bang times, and the energy downshift in the proton spectra in the rugby hohlraums. Postshot numerical simulations that include an assumed 15% energy loss on the inner cones due to backscatter were found to be in very good agreement with all observations.

Future work with rugby hohlraums needs to address the relatively higher backscatter, which partially offsets the drive enhancement. A number of techniques can be investigated to reduce the level of backscatter. Beam smoothing either by spectral dispersion or polarization rotation can be implemented, Boron doping of the Au walls has been suggested to suppress SBS in NIF hohlraums,[29] and gas-fill in the hohlraum would reduce the extent of the ablated Au plasma. Additional experiments on OMEGA can be used to assess many of these issues, but to assess the full potential of the rugby geometry, experiments on a megajoule class laser such as NIF or LMJ will be required.

ACKNOWLEDGMENTS

This work was performed under the auspices of the Lawrence Livermore National Security, LLC (LLNS), under Contract No. DE-AC52-07NA27344.

[1] J. Schein, O. Jones, M. Rosen, E. Dewald, S. Glenzer, J. Gunther, B. Hammel, O. Landen, L. Suter, and R. Wallace, Phys. Rev. Lett. **98**, 175003 (2007).
[2] P. E. Young, M. D. Rosen, J. H. Hammer, W. S. Hsing, S. G. Glendinning, R. E. Turner, R. Kirkwood, J. Schein, C. Sorce, J. H. Satcher, Jr., A. Hamza, R. A. Reibold, R. Hibbard, O. Landen, A. Reighard, S. McAlpin, M. Stevenson, and B. Thomas, Phys. Rev. Lett. **101**, 035001 (2008).

[3]D. A. Callahan, P. A. Amendt, E. L. Dewald, S. W. Haan, D. E. Hinkel, N. Izumi, O. S. Jones, O. L. Landen, J. D. Lindl, S. M. Pollaine, L. J. Suter, M. Tabak, and R. E. Turner, Phys. Plasmas **13**, 056307 (2006).
[4]M. Vandenboomgaerde, J. Bastian, A. Casner, D. Galmiche, J.-P. Jadaud, S. Laffite, S. Liberatore, G. Malinie, and F. Philippe, Phys. Rev. Lett. **99**, 065004 (2007).
[5]A. Casner, D. Galmiche, G. Huser, J.-P. Jadaud, S. Liberatore, and M. Vandenboomgaerde, Phys. Plasmas **16**, 092701 (2009).
[6]F. Philippe, A. Casner, T. Caillaud, O. Landoas, M. C. Monteil, S. Liberatore, H.-S. Park, P. Amendt, H. F. Robey, C. Sorce, C. K. Li, F. Seguin, M. Rosenberg, R. Petrasso, V. Glebov, and C. Stoekl, Phys. Rev. Lett. **104**, 035004 (2010).
[7]P. Amendt, C. Cerjan, A. Hamza, D. E. Hinkel, J. L. Milovich, and H. F. Robey, Phys. Plasmas **14**, 056312 (2007).
[8]C. Cavailler, Plasma Phys. Controlled Fusion **47**, B389 (2005).
[9]J. D. Lindl, P. Amendt, R. L. Berger, S. G. Glendinning, S. H. Glenzer, S. W. Haan, R. L. Kauffman, O. L. Landen, and L. J. Suter, Phys. Plasmas **11**, 339 (2004).
[10]E. I. Moses, Fusion Sci. Technol. **56**, 547 (2009).
[11]P. Amendt, C. Cerjan, A. Hamza, D. E. Hinkel, J. L. Milovich, H.-S. Park, and H. F. Robey, Phys. Plasmas **15**, 012702 (2008).
[12]S. W. Haan (private communication), 2008, Table of Requirements for NIF Ignition Point Design and Alternates, Version Rev. 3.11.
[13]T. R. Boehly, D. L. Brown, R. S. Craxton, R. L. Keck, J. P. Knauer, J. H. Kelly, T. J. Kessler, S. A. Kumpan, S. J. Loucks, S. A. Letzring, F. J. Marshall, R. L. McCrory, S. F. B. Morse, W. Seka, J. M. Soures, and C. P. Verdon, Opt. Commun. **133**, 495 (1997).
[14]T. Caillaud, O. Landoas, I. Thfoin, B. Rosse, M. Briat, L. Disdier, F. Phillipe, A. Casner, J. L. Bourgade, V. Yu. Glebov, F. J. Marshall, T. C. Sangster, H.-S. Park, H. F. Robey, and P. Amendt, "Neutron imaging development for inertial confinement from experiments," presented at the 51st Annual Meeting of the APS Division of Plasma Physics, Atlanta, Georgia, November 2009, Abstract No. T07.00004 (http://meetings.aps.org/link/BAPS/2009.DPP.T07.4).
[15]R. A. Lerche, D. W. Phillion, and G. L. Tietbohl, Rev. Sci. Instrum. **66**, 933 (1995).
[16]C. Stoeckl, V. Yu. Glebov, J. D. Zuegel, D. D. Meyerhofer, and R. A. Lerche, Rev. Sci. Instrum. **73**, 3796 (2002).
[17]S. P. Regan, T. C. Sangster, D. D. Meyerhofer, W. Seka, R. Epstein, S. J. Loucks, R. L. McCrory, C. Stoeckl, V. Yu. Glebov, O. S. Jones, D. A. Callahan, P. A. Amendt, N. B. Meezan, L. J. Suter, M. D. Rosen, O. L. Landen, E. L. Dewld, S. H. Glenzer, C. Sorce, S. Dixit, R. E. Turner, and B. J. McGowan, J. Phys.: Conf. Ser **112**, 022077 (2008).
[18]See National Technical Information Service Document No. DOE/SF/19460-321 (Laboratory for Laser Energetics LLE Review 80, 197, 1999). Copies may be obtained from the National Technical Information Service, Springfield, VA.
[19]See National Technical Information Service Document No. DOE/DP40200-149 (Laboratory for Laser Energetics LLE Review 45, 1, NTIS Document No. (1990). Copies may be obtained from the National Technical Information Service, Springfield, VA.
[20]C. Sorce, J. Schein, F. Weber, K. Widmann, K. Campbell, E. Dewald, R. Turner, and O. Landen, Rev. Sci. Instrum. **77**, 10E518 (2006).
[21]K. M. Campbell, F. A. Weber, E. L. Dewald, S. H. Glenzer, O. L. Landen, R. E. Turner, and P. A. Wade, Rev. Sci. Instrum. **75**, 3768 (2004).
[22]F. H. Séguin, J. A. Frenje, C. K. Li, D. G. Hicks, S. Kurebayashi, J. R. Rygg, B.-E. Schwartz, R. D. Petrasso, S. Roberts, J. M. Soures, D. D. Meyerhofer, T. C. Sangster, J. P. Knauer, C. Sorce, V. Y. Glebov, C. Stoekl, T. W. Phillips, R. J. Leeper, K. Fletcher, and S. Padalino, Rev. Sci. Instrum. **74**, 975 (2003).
[23]C. K. Li, F. H. Séguin, J. A. Frenje, M. Rosenberg, R. D. Petrasso, P. A. Amendt, J. A. Koch, O. L. Landen, H. S. Park, H. F. Robey, R. P. J. Town, A. Casner, F. Philippe, R. Betti, J. P. Knauer, D. D. Meyerhofer, C. A. Back, J. D. Kilkeny, and A. Nikroo, Science **327**, 1231 (2010).
[24]University of Rochester LLE Review Quarterly Report No. 88, p. 171 (2001).
[25]K. S. Budil, T. S. Perry, P. M. Bell, J. D. Hares, P. L. Miller, T. A. Peyser, R. Wallace, H. Louis, and D. E. Smith, Rev. Sci. Instrum. **67**, 485 (1996).
[26]S. Regan, D. K. Bradley, A. V. Chirokikh, R. S. Craxton, D. D. Meyerhofer, W. Seka, R. F. Short, A. Simon, R. P. J. Town, and B. Yaakobi, Phys. Plasmas **6**, 2072 (1999).
[27]P. Neumayer, C. Sorce, D. H. Froula, L. Divol, V. Rekow, K. Loughman, R. Knight, S. H. Glenzer, R. Bahr, and W. Seka, Rev. Sci. Instrum. **79**, 10F548 (2008).
[28]C. Stoeckl, V. Yu. Glebov, D. D. Meyerhofer, W. Seka, B. Yaakobi, R. P. J. Town, and J. D. Zuegel, Rev. Sci. Instrum. **72**, 1197 (2001).
[29]N. Meezan, S. H. Glenzer, and L. J. Suter, J. Phys.: Conf. Ser. **112**, 022022 (2008).